Forsström, Petri R.; Hovi, Aarne; Ghielmetti, Giulia; Schaepman, Michael E.; Rautiainen, Miina

Multi-angular reflectance spectra of small single trees

Published in:
Remote Sensing of Environment

DOI:
10.1016/j.rse.2021.112302

Published: 15/03/2021

Document Version
Publisher's PDF, also known as Version of record

Please cite the original version:
Forsström, P. R., Hovi, A., Ghielmetti, G., Schaepman, M. E., & Rautiainen, M. (2021). Multi-angular reflectance spectra of small single trees. *Remote Sensing of Environment*, *255*, Article 112302.
https://doi.org/10.1016/j.rse.2021.112302

Remote Sensing of Environment 255 (2021) 112302

Contents lists available at ScienceDirect

Remote Sensing of Environment

journal homepage: www.elsevier.com/locate/rse

Multi-angular reflectance spectra of small single trees

Petri R. Forsström[a,*], Aarne Hovi[a], Giulia Ghielmetti[b], Michael E. Schaepman[b], Miina Rautiainen[a,c]

[a] Department of Built Environment, Aalto University, P.O. Box 14100, 00076 Aalto, Finland
[b] Department of Geography, Remote Sensing Laboratories, University of Zürich, Winterthurerstrasse 190, 8057 Zurich, Switzerland
[c] Department of Electronics and Nanoengineering, Aalto University, P.O. Box 15500, 00076 Aalto, Finland

ARTICLE INFO

Keywords:
Goniometer
Scattering
Anisotropy
Pine
Spruce
Oak
Tree spectrum

ABSTRACT

Understanding the reflectance anisotropy of forests and the underlying scattering mechanisms is needed to improve the accuracy of retrievals of fundamental forest characteristics from optical remote sensing data. In this paper, we developed a laboratory measurement set-up for a large goniometer (LAGOS) and measured multi-angular spectra (350–2500 nm) of 18 small trees, composed of three common European tree species: Scots pine (*Pinus sylvestris* L.), Norway spruce (*Picea abies* (L.) H. Karst), sessile oak (*Quercus petraea* (Matt.) Liebl.). For all trees, we measured tree spectra in 47 view angles in the upper hemisphere. To our knowledge, this is the first study reporting multi-angular reflectance spectra of single trees. We also measured the reflectance and transmittance spectra of needles and leaves, as well as reflectance spectra of bark of the sample trees. We analyzed the spectro-directional characteristics of the trees, and the inter- and intraspecific variations of these characteristics. The anisotropy of trees was shown to be strongly asymmetrical and characteristic to species: while pine and spruce exhibited strong hotspot effects, oak showed a strong specular component. Our results indicate that simultaneous measurements of both spectral and directional characteristics of trees may enhance the discrimination of species and thus, support the retrieval of information of their biophysical properties.

1. Introduction

Currently, a wealth of satellite data is available for environmental monitoring applications. However, so far there have been only a few satellite instruments providing data on the directional scattering properties of land areas. The most well-known instruments include NASA's Multi-angle Imaging SpectroRadiometer (MISR) (Diner et al., 1998), ESA's Compact High Resolution Imaging Spectrometer (CHRIS) (Barnsley et al., 2004; Barnsley et al., 2000; Verrelst et al., 2010), and CNES's POLarization and Directionality of the Earth's Reflectances instrument (POLDER) (Deschamps et al., 1994). In addition, spectro-directional characteristics have been retrieved globally from e.g., MODerate resolution Imaging Spectroradiometer (MODIS) (Justice et al., 2002) data of large areas, and in smaller areas from multi-angular airborne (e.g., Bréon et al., 1997; Sandmeier and Deering, 1999; Lobell et al., 2002; Korpela et al., 2011; Markiet et al., 2017) and unmanned aerial vehicle (UAV) data (Roosjen et al., 2018).

Multi-angular remote sensing data have versatile uses in e.g., global monitoring of vegetation (e.g., Asner et al., 1998; Knyazikhin et al., 1998; Chen et al., 2012; Pisek et al., 2016), because the reflectance anisotropy of vegetation carries in it fundamental information on structural characteristics of canopies. Especially forest canopies have strongly anisotropic scattering patterns. The patterns have first been analyzed through radiative transfer modeling (e.g., Li and Strahler, 1992; Roujean et al., 1992; Jacquemoud, 1993; Gerard and North, 1997; Chen and Leblanc, 1997; Rautiainen et al., 2004; Kobayashi and Iwabuchi, 2008; Kuusk et al., 2014) and later on using also multi-angular remote sensing data (e.g., Lacaze and Roujean, 2001; Canisius and Chen, 2007; Rautiainen et al., 2008; Verrelst et al., 2010). In general, these studies have demonstrated that the geometric structure of canopies has a notable impact on the reflectance anisotropy of forests. More specifically, strong reflectance anisotropy has been observed in coniferous forests (e.g., Deering et al., 1999). In forest canopies, the angular effects substantially impact retrievals of biophysical variables using indices (Verrelst et al., 2008) and are slightly larger in the visible (VIS) than in the near-infrared (NIR) spectral region (e.g., Rautiainen et al.,

* Corresponding author.
E-mail addresses: petri.forsstrom@aalto.fi (P.R. Forsström), aarne.hovi@aalto.fi (A. Hovi), giulia.ghielmetti@geo.uzh.ch (G. Ghielmetti), michael.schaepman@geo.uzh.ch (M.E. Schaepman), miina.a.rautiainen@aalto.fi (M. Rautiainen).

https://doi.org/10.1016/j.rse.2021.112302
Received 9 September 2020; Received in revised form 17 December 2020; Accepted 9 January 2021
Available online 21 January 2021

2008). The hot and dark spots are the largest in the principal plane and decrease when the observation plane moves away from the principal plane (e.g., Canisius and Chen, 2007). The angular characteristics at forest stand or tree level may also be studied in the future in more detail using UAV-based remote sensing platforms. However, planning data collection by either air- or spaceborne platform relies on the availability of high-quality reference data, typically collected at ground level or modeled (Schneider et al., 2014).

Trees are typically the largest individual contributors to the spectra of a dense forest although the contribution of understory and soil layers (i.e., forest background) should not be ignored in sparser or seasonally dynamic forests (Rautiainen et al., 2011; Rautiainen and Lukeš, 2015). Although forest spectra are continuously measured by satellite instruments, reference data on the directional scattering properties of single trees are not available to date. Such multi-angular reference data, whether measured in a laboratory or in-situ, can be collected by utilizing a goniometer design that allows recording of radiation scattered by the sample in different view angles. However, goniometers are, in general, laborious and slow to use, and so far, spectro-directional characteristics have been measured only for very limited vegetation types, e.g., lingonberry and blueberry shrubs (Forsström et al., 2019), Scots pine shoots (Mõttus et al., 2012; Rautiainen et al., 2012), mosses, lichens and dwarf shrubs (Peltoniemi et al., 2005; Kuusinen et al., 2020), tree bark (Juola et al., 2020), and grass and crop species (e.g., Lunagaria and Patel, 2017; Roosjen et al., 2012; Roosjen et al., 2017). Yet due to the physical constrains of a ground-based instrument, sensor, and illumination, measuring single trees is even more tedious compared to the previously measured species that grow relatively close to the ground. Thus, laboratory goniometers capable of incorporating entire trees are very rare. At the moment, the only operational goniometer which is large enough for measuring small trees in both laboratory and field settings (Dangel et al., 2005) is the LAGOS set-up at the University of Zürich (Schopfer et al., 2008; Sandmeier and Itten, 1999). LAGOS is suitable for measuring small trees and larger single trees can be measured in nature using directional drones or cranes.

In this paper, we present the first empirical data on the spectro-directional characteristics of small single trees. We hypothesized that since tree spectra are strongly influenced by multiple scattering events within a crown, the species-specific distribution and orientation of scattering elements in tree crowns (together with leaf and bark optical properties) introduce species-specific spectro-directional characteristics for trees. To obtain the data, we developed a laboratory measurement set-up for a large goniometer and measured multi-angular spectra (350–2500 nm) of 18 small trees belonging to three common European tree species. Additionally, we measured the reflectance and transmittance spectra of needles and leaves, and reflectance spectra of bark of the sample trees. We used the data to address the following research questions: 1) what are the spectro-directional characteristics of small single trees? and 2) how large are the inter- and intraspecific variations of these characteristics? The measured data are openly available (Hovi et al., 2021 (submitted)).

2. Materials and methods

2.1. Samples

We measured spectra of evergreen conifers Scots pine (*Pinus sylvestris* L.) and Norway spruce (*Picea abies* (L.) H. Karst), and deciduous

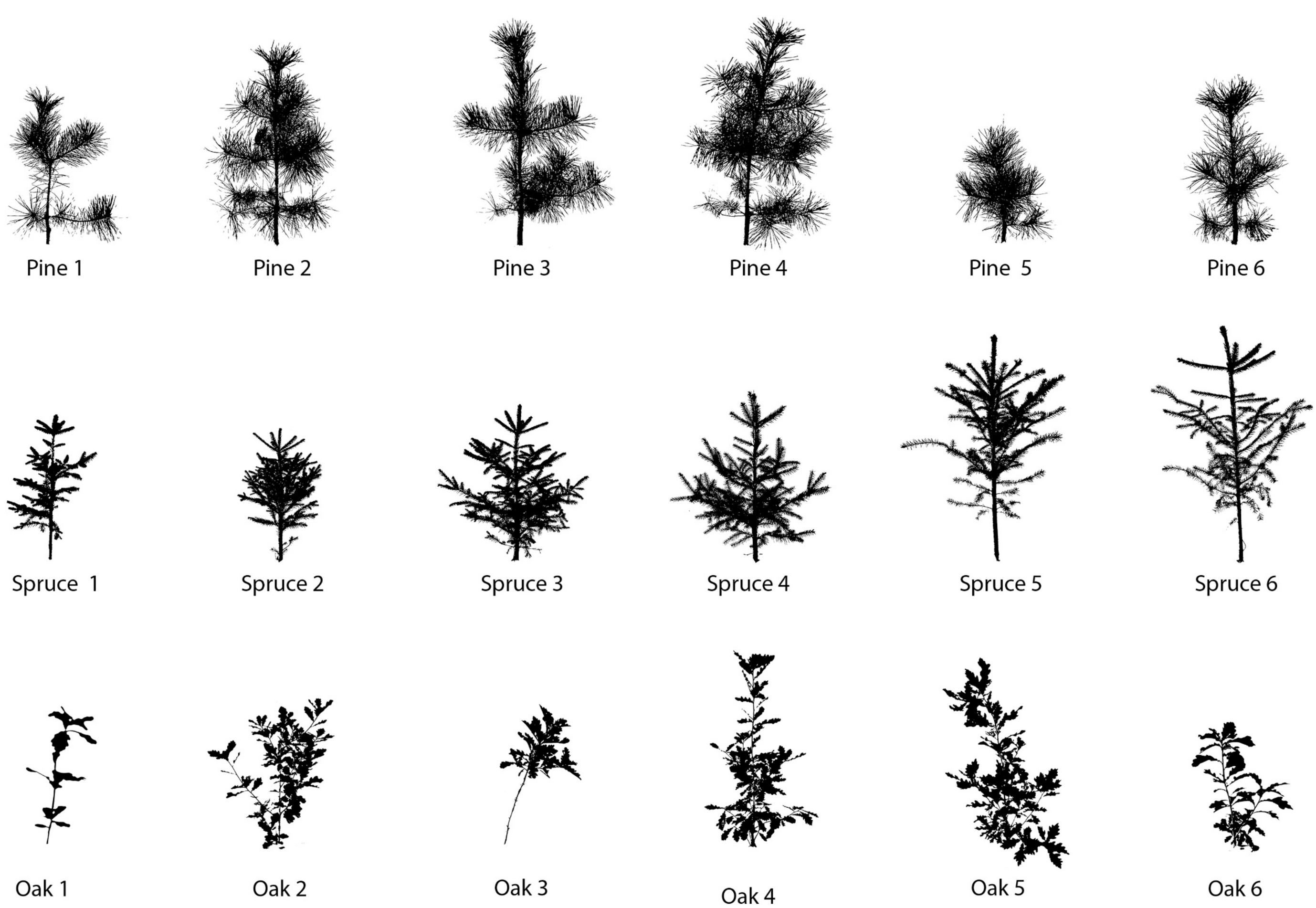

Fig. 1. Silhouettes of sample trees in comparable scale. The trees were 38–70 cm in height. See Table 1 for details on the tree species and structural characteristics.

broadleaved sessile oak (*Quercus petraea* (Matt.) Liebl.) (Fig. 1). The trees were up to 4 years old and 0.38 to 0.70 m in height, i.e., young trees. The trees were obtained from an outdoor tree nursery in Zürich between DOYs 240 and 263 in 2018. At the nursery, the trees had been grown in pots with regular watering and were exposed to direct sunlight. The study trees had healthy green leaves or needles, and intra- and interspecific variation in structure, i.e., trees were of different height, and had different crown level clumping and leaf area. (see Table 1 and Fig. 1). Variation in the structural properties of the study trees was considered an important source of natural variation of spectra. We did not select trees with heavily irregular crown shapes or strongly bent stems. The leaves of the sample trees were noted to have minor white residues of most likely calcium from the irrigation water applied at the nursery.

The sample trees were stored at the university outdoor garden in watering beds with sprinklers on top to provide automatically controlled irrigation (scheduled daily at 6 am and 6 pm). We chose the watering beds without a protective cover to keep the environmental conditions as similar as possible to those at the nursery. The growing conditions, as well as the health of the sample trees were monitored visually every day. Trees that showed visual symptoms of stress, e.g., yellowing or drooping of leaves or stem were disregarded from the measurements. Bamboo stakes were used to support the saplings and were removed only just before the spectral measurements (i.e., tree, and leaf or needle spectra), which took approximately 6 h to complete for each tree.

2.2. Measurements

The measurements were made in a dark room at the University of Zürich. The main instrument was the LAGOS goniometer in tandem with a spectrometer. The interior of the goniometer laboratory has been treated with special black paint to minimize reflections from its walls and ceiling during measurements. Also, the instrument structures, such as the stand holding the housing for the lamp, were covered with black canvases. With the aim to produce an extensive spectroscopic and structural representation of the study trees, we made a series of measurements: (i) multi-angular spectra of entire trees using the goniometer, (ii) reflectance and transmittance spectra of leaves and needles, and reflectance spectra of bark, using an integrating sphere, and (iii) crown level clumping using silhouette photographs, leaf surface areas, and leaf mass. Each measurement is described in detail in the following subsections.

Table 1
Structural parameters of sample trees. Tree species are Scots pine (*Pinus sylvestris* L.), Norway spruce (*Picea abies* (L.) H. Karst), and sessile oak (*Quercus petraea* (Matt.) Liebl.). The silhouette to total area ratio (STAR) describes crown level clumping.

Sample tree	Height [cm]	Green biomass [g]	STAR
Pine 1	50	37.3	0.170
Pine 2	62	96.8	0.138
Pine 3	69	87.2	0.153
Pine 4	70	116.6	0.145
Pine 5	38	66.0	0.114
Pine 6	50	59.1	0.135
Spruce 1	44	21.4	0.178
Spruce 2	41	38.0	0.122
Spruce 3	48	62.4	0.118
Spruce 4	53	60.4	0.139
Spruce 5	68	63.5	0.143
Spruce 6	70	36.1	0.183
Oak 1	45	4.5	0.209
Oak 2	48	20.0	0.173
Oak 3	46	9.6	0.195
Oak 4	58	21.3	0.193
Oak 5	58	23.0	0.209
Oak 6	39	14.0	0.204

2.2.1. Multi-angular measurements of tree spectra

The goniometer measurements of tree spectra were always the first in the daily measurement routine and were made directly after bringing the sample tree in the laboratory. Measuring one tree took approximately 1.5 h. The utilized system represents a traditional goniometer design in which the sensor optics of the spectrometer (ASD FieldSpec3, serial number 16006) can be pointed at the center of the goniometer from any view angle in the upper hemisphere, and the amount of scattered radiative energy recorded (Fig. 2). The measurement geometry was biconical, meaning both the incident radiation and the sensor field of view (FOV) had conical angular characteristics (Schaepman-Strub et al., 2006).

We measured spectra of trees in view zenith angles (θ) 0°, ±21.2°, ±48.6°, ±76.2°, while having the goniometer half-arc turned in relative azimuth angles (φ) 0°, 15°, 45°, 75°, 90°, 105°, 135°, 165° for each measurement (i.e., nadir was measured eight times). The azimuth 0° was in the principal plane, and positive view zenith angles indicate the backward viewing angles (towards illumination) and negative the forward viewing angles (away from illumination). The view zenith angles were chosen so that cos(θ) corresponds to nodes of Gauss-Legendre integration, which enables, when needed, a reasonably accurate approximation of the spherical integral (Atkinson, 1982), and therefore also hemispherically reflected radiation, a pre-requisite for the work performed by Hovi et al. (2020a). To summarize, there were 47 different view angles, and because nadir was measured eight times, there were in total 54 measurements per tree.

We used a bare fiber optic bundle as sensor optics for the spectrometer with an opening angle of 25°. With the fiber head at a 1.94 m distance from the goniometer center, a sample tree fit always fully in the FOV of the sensor. Before and after measuring all spectra of a tree, we took three averaged spectral reference readings from a diffuse (20 × 20 cm) Labsphere Zenith Lite™ 95% reflectance panel, placed in the center of the goniometer. The reference readings were used to convert the spectral digital number (DN) data to a meaningful reflectance quantity, as well as to validate the temporal stability of the light source during the measurements. In all view angles, we saved one averaged spectrum per 10 measured spectra, using a 2.18 s integration time. The spectrometer and the light source lamp were allowed to warm-up at least 0.5 h before the measurements. A laptop computer with ASD RS3 software was used to save the spectra.

As a light source, we utilized a broadband 1000 W tungsten-halogen lamp with a Thermo-Oriel housing and stabilized power supply. A Köhler illuminator with an aspherical reflector and a condenser were used to remove the effect of the lamp filament and to increase the spectral and spatial homogeneity at the illuminated spot. The light source was fixed to a sturdy metal stand with vertical, horizontal, and tilt adjustments. During the measurements, the light source was inside the goniometer half-arc structure and as close to the outer edge as possible in order to maximize the width of the light beam at the distance of a tree sample. All sample trees were fully illuminated during the measurements from a zenith angle of $\theta = +40°$, which is typical in summer time acquisitions of satellite data in the midlatitudes, with the maximum tree height still fitting inside the beam being around 70 cm. The opening angle of the light beam was 22° and the lamp filament was located 1.75 m from the goniometer center (Fig. 2).

To facilitate the measurements of tree spectra in the goniometer, we needed a non-reflective background in order to minimize the effect of stray light in the recorded signal. By stray light we refer to any signal source other than the signal originating from the tree. In our measurements, most of the stray light was assumed to originate from the illuminated fraction of the background. We constructed a 1.5 × 1.3 m wooden frame, to support a spectrally black canvas (Fig. 2). The frame had adjustable legs to allow correct vertical alignment for trees of different size. We used four different frame heights in our measurements: 60.0, 64.6, 69.2, and 73.8 cm. The height for each measured tree was selected based on tree height, so that the tree crown was fully

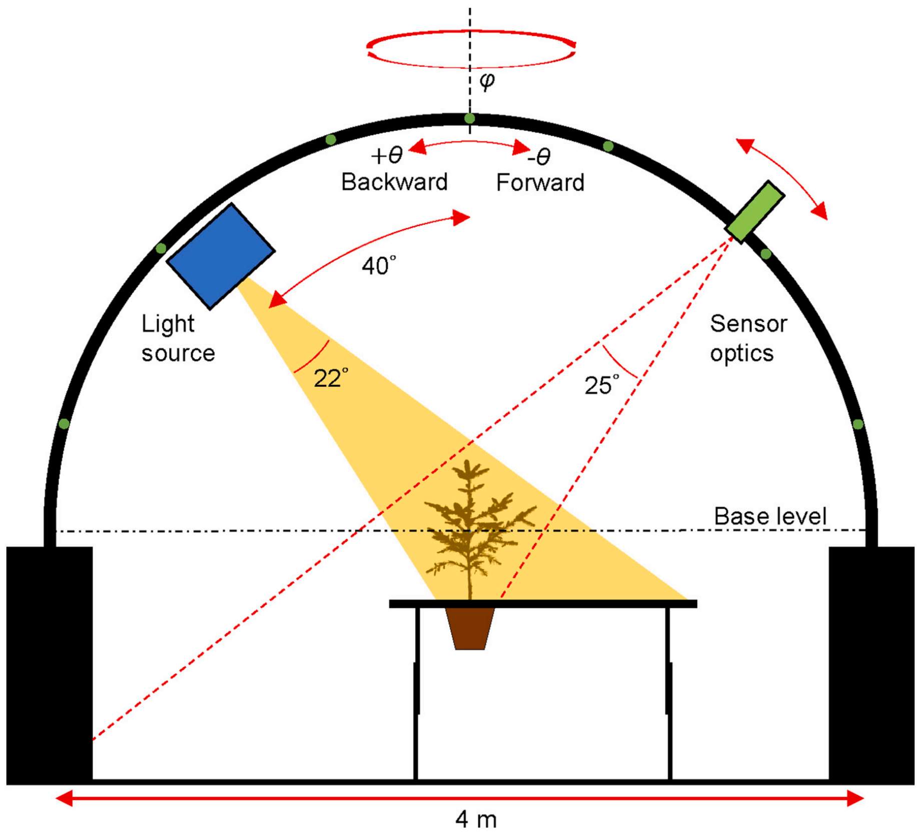

Fig. 2. Goniometer measurement set-up. The light source was fixed at +40° zenith angle (θ). During the measurements, the sensor view zenith angle ($\theta = 0°$, ±21.2, ±48.6°, ±76.2°) and sensor view azimuth angle ($\varphi = 0°$, 15°, 45°, 75°, 90°, 105°, 135°, 165°) were altered.

illuminated, but the tree pot was covered by the canvas (Fig. 2). The canvas (Sunbrella® Solid VV M100) is composed of acryl fiber, and we selected it from several tested options, because it was the darkest material available at a reasonably affordable price. The canvas was large enough to cover the horizontal projection of the light beam at the measurement spot. Thus, the light beam formed an ellipse-shaped illuminated area on the background. The directional-hemispherical reflectance factor of the canvas was 0.013–0.02 over the whole spectral range 350–2500 nm (Fig. A1). In preliminary tests outdoors, under clear-sky conditions and using a spectrometer with conical view geometry, we noticed some specular behaviour, i.e., signal from the canvas increased towards the extreme forward scattering angles. However, the amount of stray light depended not only on the reflectance of the background, but also on how large fraction of the illuminated background was in the spectrometer's FOV (see Fig. 2). The stray light signal was measured from the canvas at all view angles, separately for all four frame heights. The relative fraction of stray light (compared to the signal from the tree) peaked at regions where the tree's reflectance was low, being on average 61% at 400 nm, 39% at 660 nm, and 52% at 1930 nm. Stray light was removed during data processing steps (Section 2.3.2.3).

A tree was positioned in the goniometer through a slit cut in the black canvas and aligned to the measurement spot at the goniometer center using a projected laser dot directly in nadir. The middle point between trunk base and crown tip was aligned with the base level of the goniometer (Fig. 2). Before the measurements, the slit in the canvas was sealed to hide the pot and the supporting structure.

2.2.2. *Silhouette area photography*

After the tree spectral measurements, the sample trees were photographed in all 47 view angles of the spectral measurements, and also in the direction of the illumination. Projected silhouette areas of trees in the aforementioned view angles were calculated from the photos, and were used (i) to normalize the measured spectra to the amount of radiation intercepted by the tree crown, and (ii) to calculate a structural parameter that quantifies crown level clumping, i.e., the silhouette to total area ratio (STAR) (Stenberg et al., 2014). We explain the calculation of silhouette areas in Section 2.3.1, the processing of tree spectra in Section 2.3.2, and the calculation of STAR in Section 2.3.4. STAR for each tree is reported in Table 1.

We used a digital camera fixed next to the spectrometer sensor optics in the goniometer half-arc and pointed it towards the center of the goniometer. The camera had an adjustable zoom lens which was fixed at 45 mm focal length. The camera shutter was triggered remotely from the ground. We first took photos of a checkerboard pattern at the center of the goniometer and used Matlab Computer Vision Toolbox™ to solve the intrinsic and extrinsic camera parameters (i.e., focal length, lens distortions, and exact position and orientation of the camera at each viewpoint). During the silhouette area photography, a white canvas was placed behind the tree to increase contrast between the tree and the image background. The canvas was illuminated from the sides to minimize shadows. This was important since the silhouette areas were extracted from the photos using an automated binary thresholding method (see Section 2.3.1). When taking a photo in the direction of illumination, the lamp was moved downwards so that it did not obstruct the FOV of the camera.

2.2.3. *Structural characteristics of trees and optical properties of leaf and bark*

Leaf optical properties (i.e., reflectance and transmittance) were measured for each sample tree. We used an ASD RTS-3ZC integrating sphere with an ASD FieldSpec3 spectrometer (serial number 16007) to record the spectra (350–2500 nm) (Fig. 4). The methods were destructive and thus, the leaf level measurements were made after the measurements of tree spectra and silhouette photography. We applied the same measurement method and protocol for both leaves and needles as described for a single integrating sphere by Hovi et al. (2020b), except that we used slightly thicker needle carriers (0.8 vs 0.3 mm). We aimed for random leaf sampling, and always picked the leaf and needle samples from different heights and sides of the tree. We measured three samples of leaves or needles for each tree. By a needle sample we refer to a measurement of several pine or spruce needles in the needle carrier, while for oak, one spectral sample means a measurement from a single, spatially homogeneous spot on the surface of a leaf. The spectra of needles were measured from the needle center for pines and closer to the needle tips for spruce. This was because spruce needles needed to be placed in the carrier in two rows, because they were shorter than the diameter of the sample port of the integrating sphere (15 mm). To ensure comparability of data between the leaf and needle measurements, we used the same needle carriers for both. Measurements of leaf optical properties took approximately 1 h for a tree.

One sample tree per species was also measured for bark reflectance using the same measurement method and protocol as for leaves. Bark was peeled from the tree trunk (three samples per tree) using a sharp knife and placed flat in the needle carrier, with the outer bark surface towards the light. Bark samples were measured only for reflectance of outer surface since the transmittance of woody parts of a tree can be expected to be very close to zero.

We made direct measurements of tree height using a rigid measurement tape, and recorded fresh leaf mass for each tree (Table 1). Additionally, we calculated the leaf mass to leaf area conversion factors. These parameters were used in estimating the total leaf area for each tree and for calculating STAR (Table 1).

For determining leaf mass, we picked all needles and leaves, and weighed them using a laboratory grade scale. A smaller set of foliage from each tree (1 g and 10 g, i.e., approximately 150 needles, for pine and spruce needles, respectively, and 5 g for oak leaves) was picked to solve the conversion factor of leaf mass to projected area. The leaves or needles of this subset were weighed, and the projected area was determined by scanning the leaves and needles in a digital film scanner (Epson Perfection V550) and by applying a binary thresholding to the scanned silhouette images. For conifers, an additional small subset (10 needles) was taken for determining the projected area to total surface area conversion factor. In this subset, measurements of projected area using the film scanner, and outer dimensions (i.e., length, breadth, thickness) of the needles using a digital caliper were made.

2.3. Data processing

2.3.1. Silhouette areas of trees

The photos of sample trees (Section 2.2.2) were thresholded by applying an automatic method (Otsu, 1979) to the blue channel to yield binary black-and-white images. Before thresholding, manual selection was made by drawing a polygon around the tree to delineate areas in the photos that contained only tree and white background. The silhouette area of a tree was calculated from the obtained images by multiplying the number of black (tree) pixels with the area of a single pixel projected at the distance of the tree crown center.

2.3.2. Estimates of directional scattering coefficients of trees

2.3.2.1. Equation for directional scattering coefficient. The data from the goniometer measurements (Section 2.2.1) and silhouette images (Section 2.2.2) were processed into estimates of directional scattering coefficients (DSC, [sr^{-1}]). We define DSC as the fraction of intercepted radiation scattered into a unit solid angle around view direction vector Ω. The DSC was selected over the more common bidirectional reflectance factor (BRF), because a tree is not a surface, but rather scatters spherically in all directions. If direct comparison with remote sensing data is desired, an estimate of a tree's BRF can be obtained from the data (Hovi et al., 2021 (submitted)) by multiplying DSC with π. In addition, ratio of DSC to that of an ideal diffuse (spherically scattering) object can be obtained as DSC / (1 / 4π) = (4π × DSC). The processing is explained below. For derivation of equations, details of stray light correction, and discussion on measurement uncertainties, the reader is referred to Hovi et al. (2020a). DSC is wavelength-dependent, but the wavelength discriminator is omitted in the following formulae for the sake of clarity. DSC for a given Ω was computed as

$$\mathrm{DSC}_{tree}(\Omega) = \frac{\mathrm{DN}_{tree}(\Omega)}{\mathrm{DN}_{\mathrm{WR}}} \times \frac{S_{\mathrm{WR}}cos40^{\circ}}{S_{tree}(\Omega_i)} \times \frac{R_{\mathrm{WR}}cos0^{\circ}}{\pi} \times \frac{f_{\mathrm{WR}}}{f_{tree}(\Omega)}, \tag{1}$$

where $\mathrm{DN}_{tree}(\Omega)$ and $\mathrm{DN}_{\mathrm{WR}}$ are the measured signals from the tree and white reference, $S_{tree}(\Omega_i)$ is the silhouette area of the tree in the direction of illumination [m^2], S_{WR} is the area of the white reference panel [m^2], and R_{WR} is the reflectance factor of the white reference panel. Eq. 1 was derived from the measurement equations that describe mathematically the signals observed when measuring the white reference panel and a tree, respectively. All DN values are assumed free from stray light. Stray light correction is explained in Section 2.3.2.3. In order to take into account the different amount of radiation intercepted by the tree and the white reference panel, Eq. 1 computes the ratio of signals from the tree and the white reference panel and normalizes the result with the ratio of their silhouette areas in the direction of illumination. The result is brought into a physical scale by multiplying it with the DSC of the white reference panel, which for a Lambertian surface is $R_{\mathrm{WR}}\cos\theta / \pi$. Finally, the result is multiplied with the correction factor for the point-spread-function (PSF) of the detector ($f_{\mathrm{WR}} / f_{tree}(\Omega)$), derivation of which is explained in detail in Section 2.3.2.2. Note that Eq. 1 is for direct illumination only, i.e., the silhouette areas of the white reference panel and the tree (second term on the right-hand side), and thus the interception of incoming radiation, are computed using fixed illumination angle (here zenith angle of 40°). The equation could be adapted to outdoor measurements as well, by taking into account that some fraction of incoming radiation is diffuse. This requires that multiangular tree silhouettes are available (as in our study), thus enabling to compute the diffuse interception of the tree, and that the ratio of diffuse to total radiation and angular distribution of diffuse radiation are known.

2.3.2.2. Point-spread-functions of the spectrometer. The FOV of the spectrometer had a nominal opening angle of 25°. In reality, the sensitivity of the spectrometer's detector decreases gradually towards the edges of the FOV, which means that the signal from a target is dependent on the location of the target inside the FOV. For example, for a large tree (e.g., 70 cm in height) viewed at a zenith angle of 76.2°, the signal originating from the treetop was already within the low sensitivity area. Thus, the signal was lower than what would be observed by a detector that has equal sensitivity across entire FOV (i.e., an isotropic detector). The correction factor $f_{\mathrm{WR}} / f_{tree}(\Omega)$ was introduced to account for this. The terms f_{WR} and $f_{tree}(\Omega)$ are factors calculated for the white reference panel and for the tree, respectively. They describe the fraction that the recorded signal represents, compared to a signal observed from the same target by an isotropic detector, and were obtained by weighting the silhouette images of the tree and white reference panel, respectively, with the PSF of the detector. The PSF was obtained from measurements of a small Spectralon® panel, taken so that the panel was placed at different locations inside the FOV, and by fitting an asymmetric 2D Gaussian function in the measurements. This was done separately for each of the three detectors of the spectrometer, i.e. VNIR (350–1000 nm), SWIR1 (1001–1800 nm), and SWIR2 (1801–2500 nm). Applying the correction factors $f_{\mathrm{WR}} / f_{tree}(\Omega)$ slightly reduced the jumps in tree spectra observed between different detectors of the spectrometer. These jumps, measured in relative terms [%] (i.e., (DSC(band 2) - DSC(band 1)) / DSC(band 1) * 100%), were reduced from −9.5 ± 9 (mean ± standard deviation) to −7 ± 7.9 at 1001 vs. 1000 nm, and from −3 ± 3.9 to 0.8 ± 3.5 at 1801 vs. 1800 nm. The remaining jumps indicate that the correction was not perfect. This is most probably because the correction assumes that the tree is equally bright in all parts. In reality, the side of the tree that was closer to the lamp received the largest amount of radiation and was therefore the brightest.

2.3.2.3. Removal of stray light. Because the stray light fraction was known from measurements (Section 2.2.1), stray light [DN] could be calculated for any view angle based on a measurement of the white reference panel. The challenge was that the tree (or white reference panel) and its shadow covered partly the illuminated background and thus, obscured some fraction of the stray light. Therefore, for an accurate stray light removal, we used the formula

$$DN = DN_{total} - bDN_{stray}, \quad (2)$$

where DN is the signal free from stay light, DN_{total} is the original DN value measured, DN_{stray} is the stray light signal without the presence of the tree or white reference panel, and b is the fraction of stray light not obscured by the tree or white reference panel. Calculation of b was done for each of the detectors of the spectrometer separately. For each tree and view angle, b was calculated by utilizing the silhouette images taken from the view angle and the direction of illumination (Section 2.2.2), as well as modeled PSF of the spectrometer and irradiance distribution of the light beam. The latter was obtained using the red channel of RGB photographs of the light beam on the black background. The image data were linearized (i.e., gamma correction removed) before using them in modeling the irradiance distribution. First, the irradiance distribution of the light beam and PSF of the spectrometer were projected on the image taken from the view angle (Fig. 3a–b). Second, a hypothetical stray light signal without a tree was computed by multiplying the PSF with the irradiance distribution of the light beam. The result is shown as the red-yellow area in Fig. 3c. Third, the tree and its shadow were obtained from the silhouette images and were then projected on the same image (Fig. 3a–c) to compute the fraction of the stray light that was not obscured by the tree and its shadow. The calculation of b was performed similarly for the white reference panel, except for that the automatic image thresholding was not applicable, and silhouette and shadow of the panel were manually measured from images of the white reference panel at nadir.

In wavelength regions where the tree was dark and the ratio of stray light (bDN_{stray}) to signal from the tree (DN) was high (e.g., on average 61% at 400 nm, 39% at 660 nm, and 52% at 1930 nm), the stray light correction using Eq. 2 prevented negative DSC(Ω) values and resulted in an average increase of DSC(Ω) by 59% at 400 nm, 30% at 660 nm, and 68% at 1930 nm, compared to a simple stray light correction, i.e. b set to 1.

2.3.3. Leaf and bark spectra

The directional-hemispherical reflectance and transmittance factors (referred as simply reflectance and transmittance) of leaves and needles, as well as reflectance of bark were computed with commonly used formulas for single integrating sphere (Eq. 37 and Eq. 38 in Hovi et al., 2020b). Processing of needle spectra required the retrieval of the gap fractions of the needle sample within the collimated light beam. These were obtained by scanning the needle carrier with needles in it, using a digital film scanner, and by applying a threshold to the obtained 8-bit grayscale images within the area of the light beam to separate the needles from the background. For needles of pine and spruce, the threshold value (202 for pine, 187 for spruce) was selected so that, when the resulting gap fraction was applied in data processing (Eq. 38 in Hovi et al., 2020b), the mean needle transmittance at 410–420 nm was 0.021 for pine, and 0.039 for spruce. These values were obtained in a separate measurement campaign in 2019, for the same species but growing in Finland. In that campaign, the gap fractions of the needle samples were obtained directly through measurements in the integrating sphere, by painting the illuminated side of the needles black, thus ensuring that the measured transmittance signal was only due to the transmission through the gaps between needles (Daughtry et al., 1989). An accurate estimate of needle transmittance could then be derived from measurements made before painting, because the gap fraction was known. In addition, we applied an empirical transmittance correction that adjusted all transmittance spectra 5.5% downwards. It was taken from the measurements made against a trusted reference method in Hovi et al. (2020b). The correction ensured that leaf and needle albedos did not exceed unity. Leaf and needle albedos were computed as the sum of reflectance and transmittance, and bark albedo was assumed equal to bark reflectance. The processed leaf, needle, and bark albedos are shown in Fig. 4 and used in the interpretation of our results.

2.3.4. Silhouette to total area ratio (STAR) of trees

For each tree, leaf and needle mass were converted to total leaf (or needle) area, using two linear conversion factors: mass to projected area and projected to total surface area. The former was determined from the subset of leaves (needles) that had been scanned and weighed. The latter for coniferous needles was determined from the subset of needles that had been scanned and measured for needle dimensions. In order to compute the total needle area from the measurements of needle dimensions, the shape of pine needles was assumed as semi-fusiform (Eq. 7 in Flower-Ellis and Olsson, 1993), and that of spruce needles was assumed as parallelepiped (Eq. 9 in Sellin, 2000). For broadleaved trees, the total leaf area was obtained simply by multiplying the projected area by a factor of two. Finally, STAR was computed for each tree as the ratio of the spherically averaged tree silhouette area to total leaf (or needle) area.

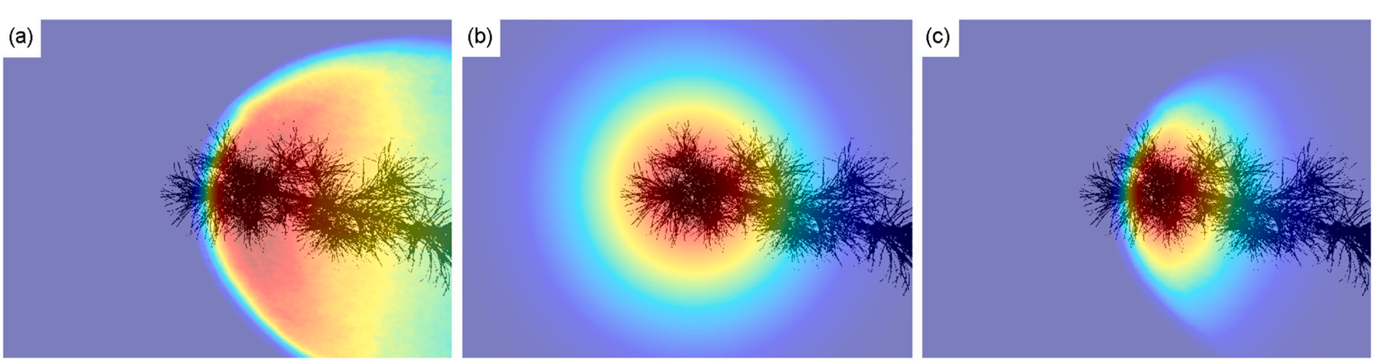

Fig. 3. Illustration of the computation of fraction of stray light not obscured by the tree and its shadow in the goniometer measurements for one view angle (view azimuth angle 165°, view zenith angle 21.2°, light originates from west-northwest direction). All images show silhouette and shadow of the tree projected onto a plane perpendicular to the given viewing direction (black areas). Sub-figure (a) illustrates irradiance distribution of the light beam, (b) the point-spread-function (PSF) of the spectrometer, and (c) the product of irradiance distribution and PSF. For details of stray light correction, the reader is referred to Hovi et al. (2020a).

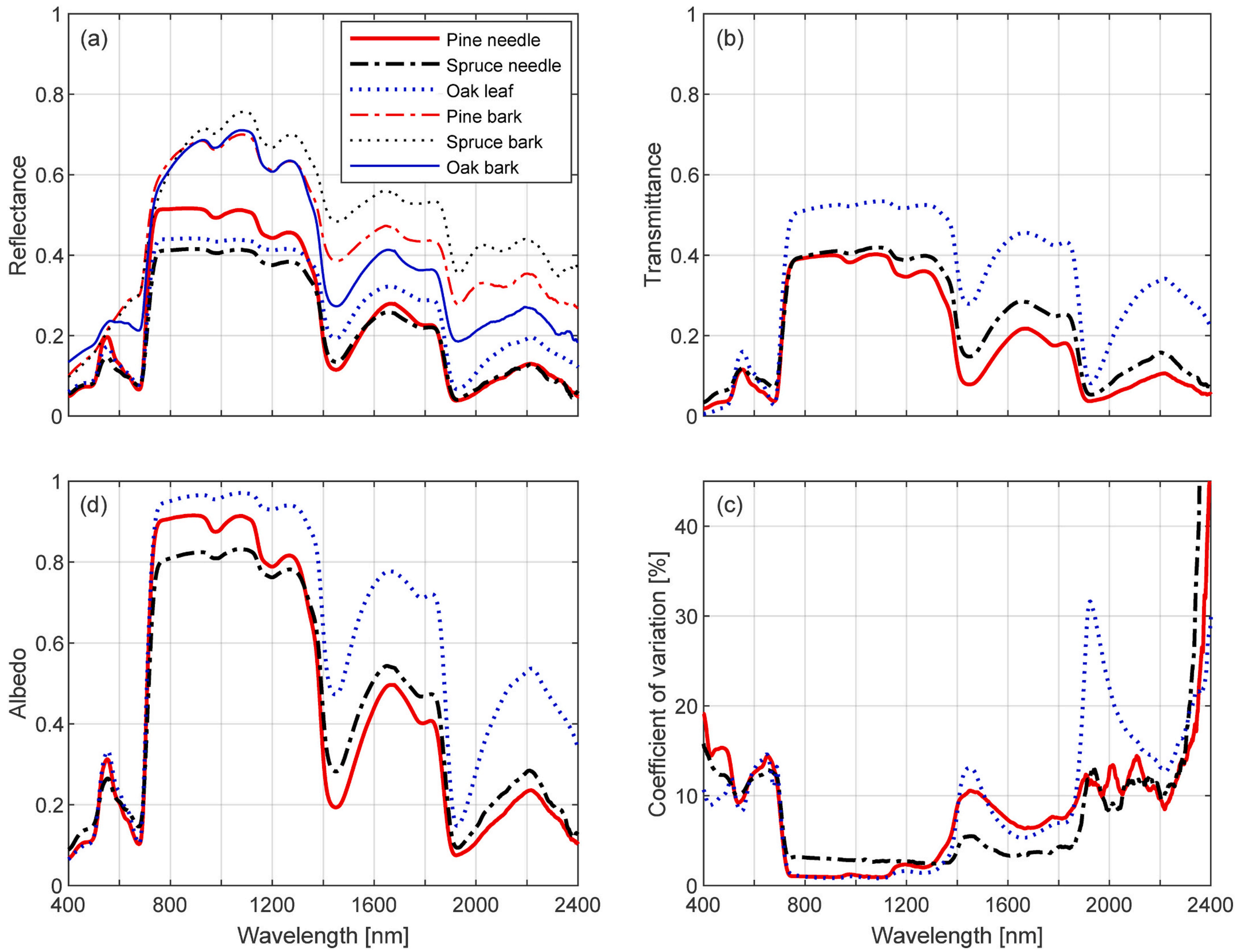

Fig. 4. Needle, leaf, and bark mean reflectance spectra (a), needle and leaf mean transmittance spectra (b), and corresponding albedo spectra (c). Coefficients of variation (d) are for albedos, and are calculated using the mean spectrum for each individual tree, i.e. they measure the intraspecific variation between trees. Leaf and needle reflectance and transmittance are means from both sides of the leaves, and bark reflectance is of the external surface. NDVI was 0.76 for pine needles, 0.68 for spruce needles, and 0.69 for oak leaves, based on reflectance spectra (a) in red (665 ± 5 nm) and NIR (865 ± 5 nm) wavelengths. The spectra were smoothed to remove spectral noise using a second order Savitzky-Golay filter with 31 nm (350–1680 nm) and 81 nm (1681–2400 nm) frame lengths. The noisiest wavelengths below 400 nm and above 2400 nm are excluded. (For interpretation of the references to colour in this figure legend, the reader is referred to the web version of this article.)

3. Results

We present the spectra of the sample trees and analyze inter- and intraspecific variations in their spectro-directional characteristics. We show data in full spectral resolution (400–2400 nm) in the conventional nadir, or near-nadir view angle of most satellite sensors, and visualize the multi-angular scattering patterns of each species in six wavelength regions commonly used to study vegetation characteristics from multispectral satellite data. Furthermore, we examine the spectral characteristics and anisotropy of trees in the principal plane and cross-plane, sometimes referred to as the orthogonal plane, and report the normalized difference vegetation index (NDVI) (Rouse et al., 1974) at leaf and tree level.

In nadir, all species exhibited spectral characteristics expected for healthy green vegetation (e.g., Gates et al., 1965; Knipling, 1970): relatively low scattering in VIS (400–700 nm), high scattering in NIR (750–1300 nm), and decreasing scattering in the shortwave infrared region (SWIR) (>1300 nm) (Fig. 5a). These same basic spectral characteristics were observed in the spectral albedos of individual leaves and needles of the sample trees (Fig. 4).

In general, spruce and oak scattering was notably stronger compared to pine in nadir (Fig. 5a): oak exhibited the highest DSC in blue (~450 nm) and green spectral regions (~560 nm), while spruce DSC was the highest in the red region (~660 nm). Pine was notably darker than oak and spruce in the red region (34% and 24%, respectively). In a narrow green spectral region (~550 nm) pine was slightly brighter than spruce (1%), while still being considerably darker than oak (15%). Overall, spruce and oak spectra were fairly similar in VIS and NIR (DSCs within 5% of each other), while less so in SWIR where oak was notably (39%) brighter than spruce. Pine, on the other hand, scattered less than spruce and oak in NIR (23% for both), as well as in SWIR (30% and 49%, respectively). In the red-edge, moderate interspecific variation was observed between the broadleaved and coniferous species: oak was brighter than pine and spruce (21% and 16%, respectively) between 710 and 720 nm. Additionally, in the longer wavelengths of the red-edge, where the spectral curve transitions into the NIR plateau, the transition was sharper for oak and pine than for spruce.

In nadir, the spectral absorption effect by water contained in the

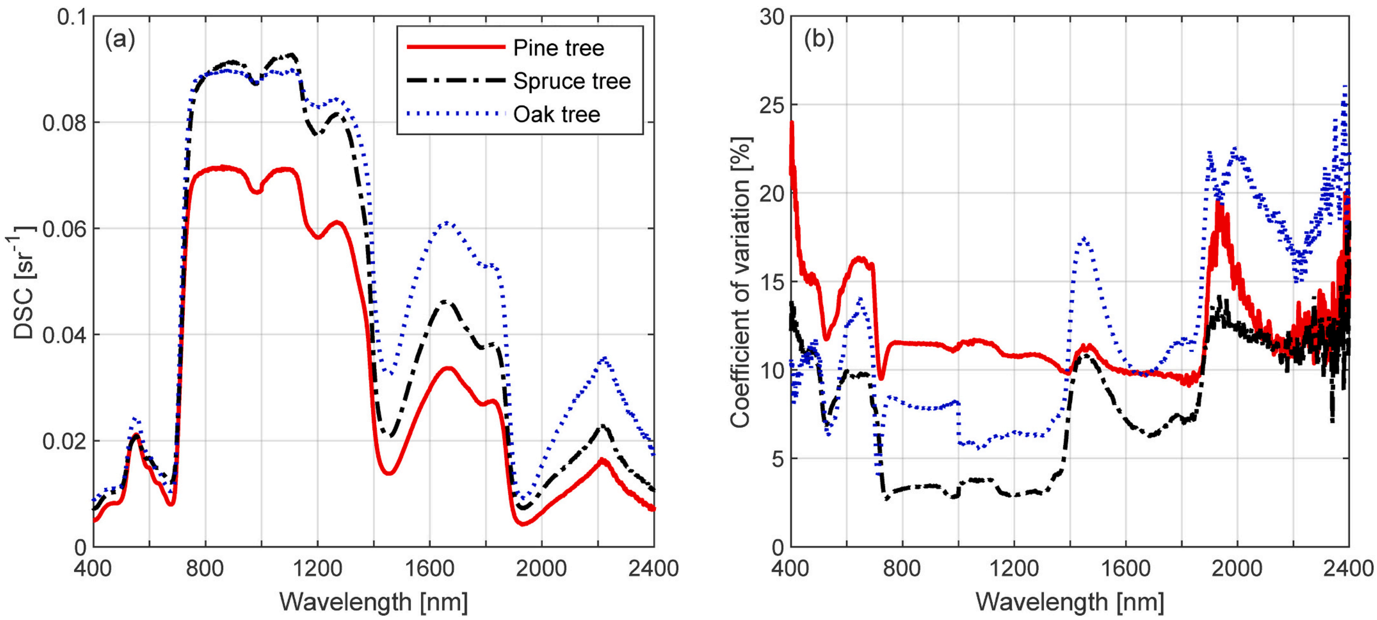

Fig. 5. Mean directional scattering coefficient (DSC) (a) and corresponding coefficient of variation (CV) (b) per tree species in nadir. CV was calculated using mean nadir spectrum for each individual tree, i.e., it measures the intraspecific variation between trees. NDVI was 0.78 for pine, 0.76 spruce, and 0.78 for oak, based on mean DSCs (a) in red (665 ± 5 nm nm) and NIR (865 ± 5 nm) wavelengths. The noisiest wavelengths below 400 nm and above 2400 nm are excluded.

trees was evident: clear absorption peaks were noted in water absorption regions in NIR and SWIR for all species (Fig. 5a). To analyze the interspecific differences in water sensitivity, we compared the estimated mean DSC of each species at a wavelength of high reflectance (865 nm) (i.e., low sensitivity to spectral effects of water) to those at the water absorption peaks (i.e., 970 nm and 1020 nm in NIR, and 1450 nm and 1930 nm in SWIR). In NIR, these ratios were similar for all species (i.e., the ratios varied from 1.00 to 1.06). In SWIR, however, there were considerable differences between the species: the ratio at 1450 nm was 5.1 for pine, 4.3 for spruce, and 2.7 for oak, and at 1930 nm it was 16.9 for pine, 12.4 for spruce, and 9.8 for oak, i.e., pine and spruce exhibited larger water absorption features than oak.

The intraspecific variations in nadir DSCs, as presented by coefficients of variation (CV), showed strong spectral dependence and were different for each species (Fig. 5b). For the spectral range, where the noise was low (400–2400 nm), the mean CV was the smallest for spruce (7.7%) and somewhat larger for pine and oak (12.1% for both). Intraspecific variations were the largest in SWIR for spruce and oak, and in VIS for pine. Smallest intraspecific variations were in NIR for all species.

The multi-angular scattering patterns (Fig. 6), and the mean spectra of trees in the principal and cross-plane (Fig. 7, Fig. A2) revealed a strong dependence of scattering on the view angle. Nevertheless, the basic characteristics of vegetation spectra, recognized also at leaf level and in nadir spectra (Fig. 4 and Fig. 5) were always present. The multi-angular scattering patterns were strongly asymmetrical along the principal plane between backward and forward viewing angles (Fig. 6 and Fig. 7 left column) and symmetrical along the cross-plane between the left and right sides (Fig. 6, Fig. 7 right column). The small asymmetry noted in the cross-plane anisotropy patterns for oak (Fig. 6, Fig. 7 right column) can be a coincidence due to the relatively small number of sample trees (6), or it could be due to the measurement set-up (e.g. slight asymmetry in the spectrometer's PSF), rather than any systematic scattering characteristics of the trees. In the principal plane, all tree species were observed to scatter more backwards towards the light source ($\theta = +48.6°$, $\Phi = \pm 15°$) than forwards away from the light source. Pine and spruce had stronger hot spot effects than oak, i.e. larger increase of DSC from nadir towards the hotspot (Fig. 6, Fig. 7 left column). In forward viewing angles, however, while oak showed a strong specular component (DSC increased from nadir), pine scattering changed notably less, and spruce exhibited no such forward enhancement being increasingly darker as the view zenith angle increased (DSC decreased from nadir) (Fig. 6, Fig. 7 left column). In the cross-plane, each tree species showed a clear species-specific behaviour of scattering (Fig. 6, Fig. 7 right column): although spruce scattered strongly upwards in most of the measured wavelengths (more than pine, less than oak), its scattering decreased as the view angle was altered from nadir, as in the forward view angles. Pine scattering, on the other hand, always increased towards larger view zenith angles but was typically less than that of spruce and oak. The strongest cross-plane scattering was observed for oak: DSC first increased when moving away from nadir and then decreased at the maximum view zenith angle ($\theta = +76.2°$).

Although the highest DSC was always observed close to the hot spot for all species, the level of DSCs in other view angles varied (Fig. 6 and Fig. 7). To further compare the differences in reflectance anisotropy between tree species, we computed backward to forward scattering ratio. It was computed as mean of all backward DSCs divided by mean of all forward DSCs (excluding DSCs in view angles in the exact cross-plane ($\Phi = 90°$) and the principal plane ($\Phi = 0°$). Spruce and pine exhibited stronger backward scattering in VIS with ratio between 1.6 and 1.7 than oak with ratio 1.1. While in longer wavelengths, the ratio decreased for spruce and pine to 1.3 in NIR, for oak it slightly increased in NIR to 1.2.

4. Discussion

4.1. Relationships between tree structure and spectra

Tree spectra (DSC) depended strongly on view angle and wavelength. The spectro-directional characteristics were different for the three species, thus implying that pine, spruce, and oak could be discriminated from each other in the forward viewing angles and in the cross-plane.

While all three species scattered the incident light strongly backwards, pine and oak showed also scattering peaks in the forward and cross-plane viewing angles. The spectral anisotropy of trees was always the largest in the principal plane and in the visible spectral region. Oak had the most notable specular reflectance component while spruce was the darkest in the forward viewing angles. Next, we will discuss the

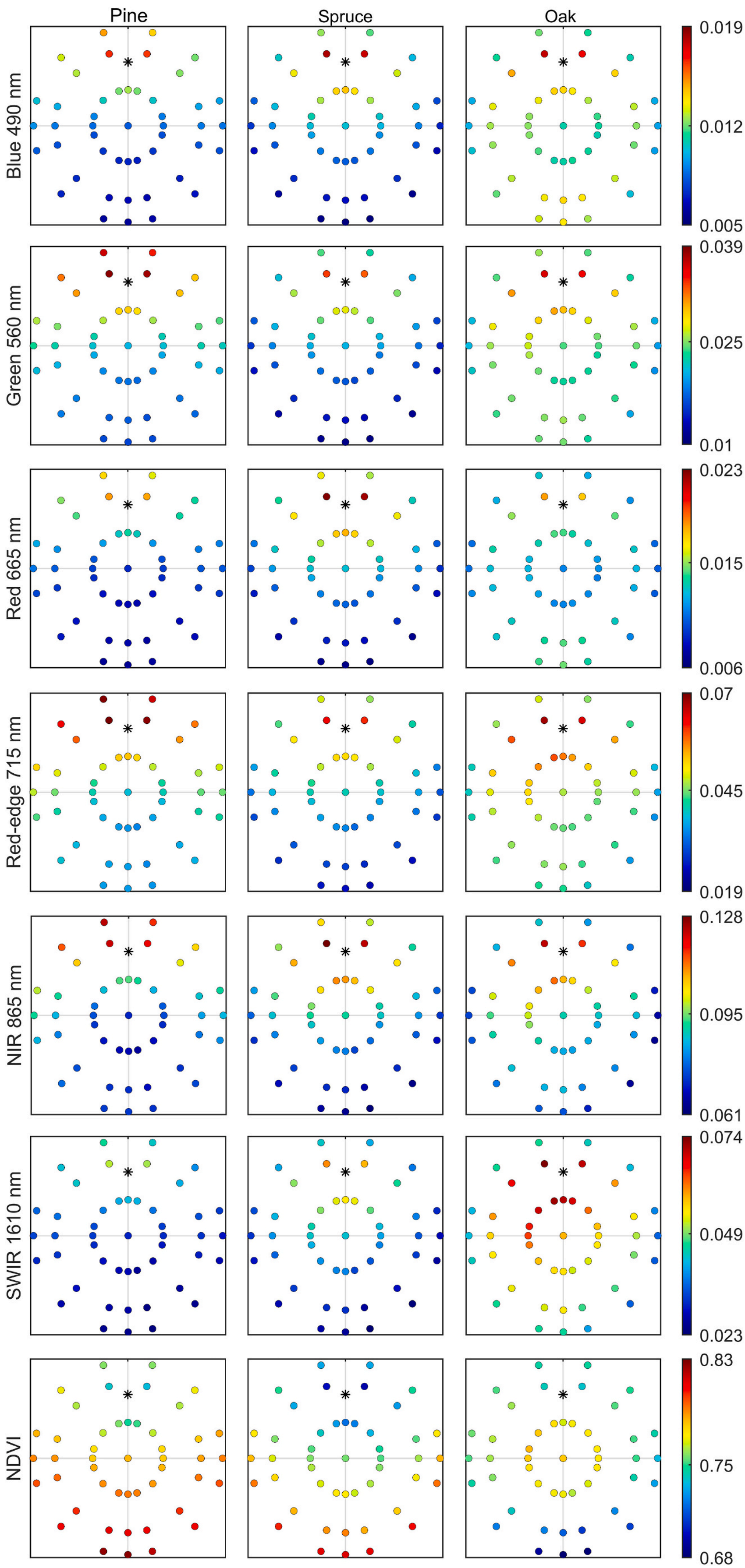

Fig. 6. Mean multi-angular scattering patterns of pine, spruce, and oak (columns) in six wavelengths commonly used in satellite sensors (±5 nm bands) (six top rows) and as NDVI (bottom row). The reflectance quantity is directional scattering coefficient (DSC) [sr^{-1}]. The colour scale covers the entire data range in each wavelength and NDVI. Nadir is at the center of each sub-figure. Off-nadir view zenith angles (±76.2°, ±48.6°, ±21.2) are indicated by the data points radiating outwards from the center points, while the view azimuths angles (0°, 15°, 45°, 75°, 90°, 105°, 135°, 165°) are distributed radially around the center. The black asterisk symbol represents the light source at a view zenith angle +40°.

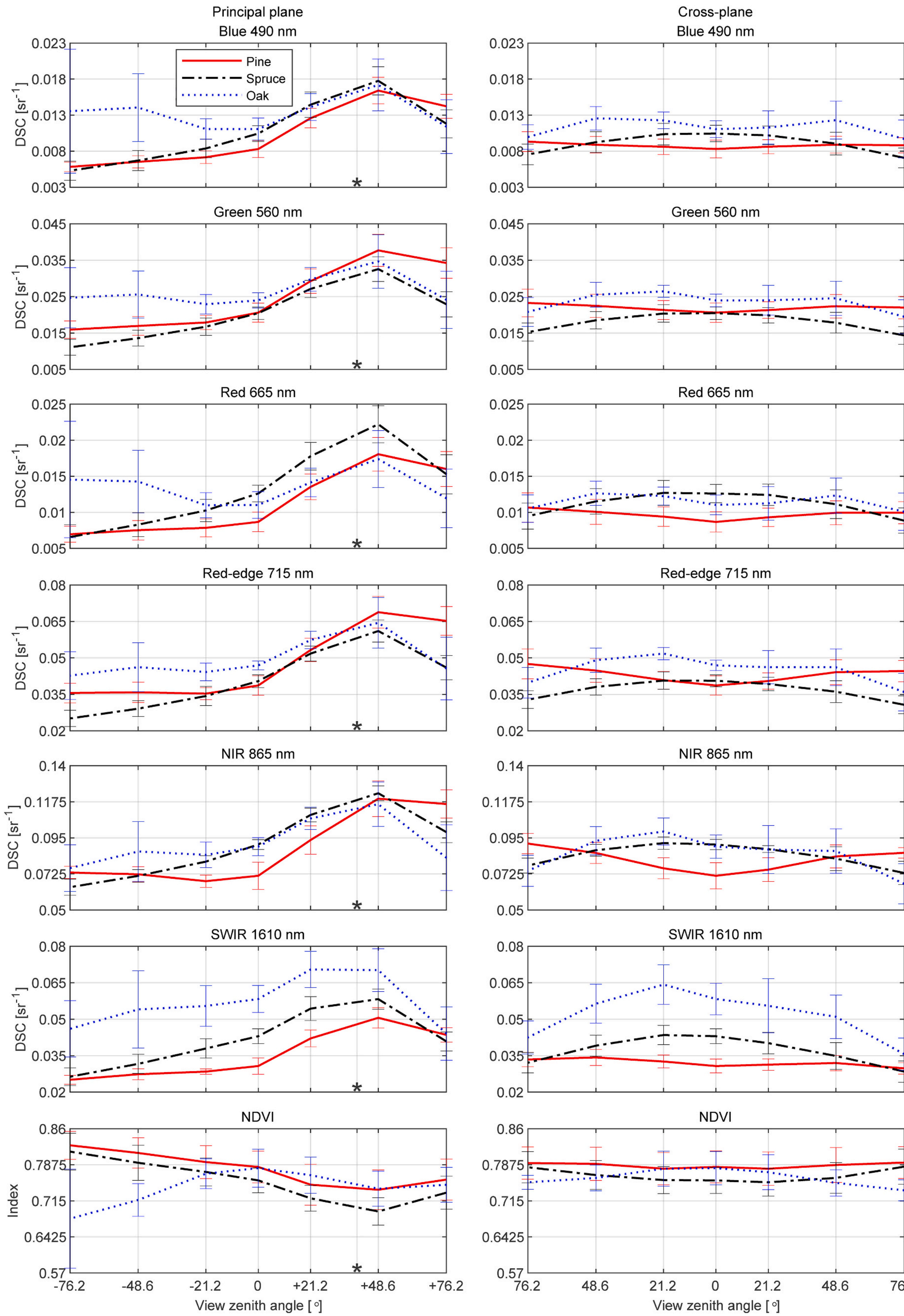

Fig. 7. The angular distribution of mean directional scattering coefficient (DSC) [sr^{-1}] for pine, spruce and oak in the principal plane (left column) and in the cross-plane (right column) at six wavelengths (±5 nm bands) (six top rows) and as NDVI (bottom row). Error bars correspond to standard deviations. Scaling of y-axes differ between sub-figures. The black asterisk symbol represents the light source at view zenith angle +40° in the principal plane.

reasons for these observed differences between the study species.

The leaf level albedos (Fig. 4) could be used to explain the interspecific differences in nadir tree spectra only partially (Fig. 5). While pine trees were darker than spruce trees in almost all wavelengths in nadir, pine needles scattered notably more than spruce needles throughout the NIR region and in green. Elsewhere in the spectrum, the order of conifer trees followed that observed at needle level. Similarly, oak leaf and tree level spectra exhibited differences in VIS: oak leaves scattered relatively less in red and more in blue compared to conifer needles, but the opposite behaviour was observed at tree level. In VIS, oak leaves were more similar to pine needles than to spruce needles. Previous studies of leaf and needle albedos have reported similar spectral characteristics for leaves and needles of different tree species (e.g., Hovi et al., 2017a) but, to-date, there is no systematic comparison of tree level spectra of different species. Comparison of NDVIs, based on leaf reflectance and tree DSC in nadir, revealed that while NDVI was always large (from 0.68 to 0.78), it was larger at tree level for all species, and more similar between species at tree level than at leaf level, mostly due to the pine needles having higher NDVI at leaf level than spruce and oak.

In addition to leaf level spectral properties, we examine species-specific differences in tree structure (Table 1). We will start by looking at the two coniferous species. Even though spruce and pine had similar mean values of crown level clumping ($STAR_{spruce} = 0.147$, $STAR_{pine} = 0.143$), spruce was brighter than pine in almost all wavelengths in nadir. We speculate that the relatively open structure of pine (i.e., sparse branching pattern) resulted in more light entering deeper into the crown before interacting with either needles or woody parts, and more of the intercepted light escaping in forward and side viewing angles, and less towards nadir. Based on measurements and visual observations of the sample trees, pine needles were long and distributed in a fewer number of shoots, whereas spruce needles were small, and more tightly aggregated around a larger number of shoots and branches. We also speculate that spruce exhibits a higher amount of self-shadowing from its structural parts, effectively blocking photons from escaping the crown.

Next, we will compare results of broadleaved and coniferous species. Oak had clearly less clumping than the coniferous species ($STAR_{oak} = 0.197$). This was in line with oak being always brighter than pine, somewhat brighter than spruce in VIS and NIR, and notably brighter than spruce in SWIR in nadir. We suggest that the spectral differences between the broadleaved oak and the two coniferous species rise from the following factors: (i) the flat and more frequently horizontally oriented (planophile) oak leaves (Farque et al., 2001; Chianucci et al., 2018) scatter upwards more effectively than needles arranged on shoots, (ii) the structure (as depicted by crown level STAR) of oak trees induces a smaller amount of multiple scattering compared to the conifers, and (iii) there was less water in oak leaves compared to conifer needles. It should also be noted that the small amount of multiple scattering within oak crowns resulted in more similar leaf and tree level spectra than in spruce and pine.

The interspecific variation in the transition from the red-edge spectral region to the NIR could be related to species-specific contribution of woody parts on the overall spectra. The spectral measurements of bark reflectance (Fig. 4) were in line with our visual observations: while oak had a notable absorption peak in red and brightening in green wavelengths, spruce and pine bark reflectance increased more linearly towards longer wavelengths, due to a smaller influence of bark chlorophyll. Although all measured bark spectra were similar in the transition between the red-edge and NIR regions (725–800 nm), spruce bark reflectance was still the smallest of the three species. This might at least partly explain the differences observed in the transition region.

4.2. Measurements of spectral anisotropy of trees

Our broadleaved study species, oak, displayed large anisotropy of reflectance in the principal plane with profound scattering peaks, not only backwards, but also forwards. The strength of the specular reflectance component of oak depended on the wavelength so that in VIS, the effect was larger than in NIR and SWIR. Firstly, this was most likely due to the sparse distribution of horizontally oriented leaves in the oak crown. Secondly, it could be explained by the protective wax layer on oak leaves: in VIS, while most of the incident energy penetrates the leaf surface and gets absorbed by leaf pigments in energy conversion, some fraction is reflected specularly by the protective wax layer residing on the leaf surface (Bousquet et al., 2005). Since the scattering properties of wax itself are independent of wavelength (Bousquet et al., 2005), the spectral differences in the forward scattering component of a leaf depend mainly on the optical interactions inside the leaf: unlike energy in the visible wavelengths, a leaf efficiently diffuses NIR radiation in its cell structure, decreasing the contribution of specular scattering from the surface on the overall spectra (Bousquet et al., 2005). Thus, although the optical properties of leaves and needles are quite similar (e.g., Hovi et al., 2017a), the specular effect is stronger in broadleaved species which have horizontally oriented leaves with large surface areas. Due to the relatively large specular component and lower amount of backward scattering, oak had the smallest backward to forward anisotropy of all three species.

Spectral anisotropy measurements of single trees, as presented in this paper, pave the way for a more comprehensive understanding of how forest reflectance is formed. Similar measurements have not been previously made due to technical challenges related to e.g., developing suitable measurement (goniometer) set-ups. Thus, both the results and the measurement method presented in this paper are novel. For measuring samples with height, such as trees, the instrument design should allow enough distance between the sensor optics and the sample so that the tree is within the FOV of the sensor in all view angles. This is a major challenge since facilitating a large goniometer indoors requires a lot of resources. Moving the sensor away from the sample reduces the parallax error, arising from the physical size of the sample, and increases the accuracy of directional measurements by making the sensor aperture appear smaller to the sample. However, increasing the distance between the sensor and the sample decreases signal quality as the level of noise increases. Additionally, if a sample does not fully cover the FOV of the sensor, as was the case with our sample trees, correction for the background signal, i.e., stray light, which varies with the view angle, must be executed with care. Furthermore, defining the correct reflectance quantity for vertical samples may not be as straightforward as for samples with less height. Thus, even though goniometers offer currently the only possibility for obtaining spectro-directional data of vegetation in a controlled environment, goniometer designs are always also a compromise between feasibility and accuracy.

4.3. Links to remote sensing of forests

Overall, examination of leaf and tree spectra revealed some surprising inter- and intraspecific similarities between the two levels and can be compared with multi-angular characteristics of forest reflectance in previous studies. However, due to the diversely different structural and compositional properties, comparison of data between the two scales is not straightforward. While some similarities and differences can be identified, it should be noted that our results are for small trees, and further research would be needed on the characteristics of full-sized trees for a more comprehensive comparison. Experimentally, isolating large trees comparable to our small size tree laboratory experiment will be one of the key challenges to transfer or even scale information to larger areas.

The similarities in spruce and oak tree spectra observed in this study (Figs. 5, 6, 7) are surprising since forest reflectance in satellite and airborne images has been shown in general to be higher in NIR for deciduous forests (in summer) compared to coniferous forests (e.g., Kimes et al., 1986; Ranson et al., 1994; Bréon et al., 1997; Eklundh et al., 2003; Canisius and Chen, 2007; Rautiainen et al., 2008; Heiskanen et al., 2013; Rautiainen and Lukeš, 2015; Hadi et al., 2016). This can be explained by factors related to the absence of the natural scattering environment of the trees, i.e., the surrounding forest: (i) the overall canopy structure (e.g., spatial arrangement of trees) and thus multiple scattering as well as mutual shadowing between trees, influence forest reflectance (e.g., Li and Strahler, 1992), and make it substantially different from that of an individual tree crown, and (ii) in addition to structural and spectral properties of trees, the reflectance of a forest also depends strongly on the visibility of the understory vegetation and soil to the sensor (e.g., Rautiainen and Lukeš, 2015) which is typically largest in view angles close to nadir (e.g., Korhonen et al., 2011; Hovi et al., 2017b; Kuusk et al., 2018).

Our results can also be compared to multi-angular data from deciduous and coniferous forests at crown- (e.g., Korpela et al., 2011; Korpela et al., 2014), stand- (e.g., Kimes et al., 1986; Ranson et al., 1994; Bréon et al., 1997; Sandmeier and Deering, 1999; Canisius and Chen, 2007; Rautiainen et al., 2008) or landscape-level (e.g., Bicheron and Leroy, 2000). In general, our study corroborated findings of previous airborne- and satellite measurements: there is a strong hot spot effect in the principal plane for single trees and entire forests (e.g., Bréon et al., 1997; Sandmeier and Deering, 1999; Rautiainen et al., 2008). Similarly, in the forward view angles, deciduous canopies (e.g., Kimes et al., 1986; Bréon et al., 1997; Canisius and Chen, 2007) and single oak trees (Fig. 6, Fig. 7, left column) have now been shown to exhibit a clear scattering peak (most prominent in VIS), and coniferous canopies (e.g., Sandmeier and Deering, 1999; Canisius and Chen, 2007) along with pine and spruce trees (Fig. 6, Fig. 7 left column) have been shown to be dark at larger view zenith angles. Furthermore, the angular effects noted in the principal plane seem to decrease as a function of increasing wavelength for both forests (e.g., Sandmeier and Deering, 1999; Rautiainen et al., 2008) as well as single tree crowns (Fig. 6, Fig. 7). Our study also revealed an interesting new finding: while NIR reflectance of deciduous stands have previously been reported to be distinguishably stronger than that of coniferous stands in nadir and backwards along the principal plane (e.g., Canisius and Chen, 2007; Rautiainen et al., 2008), in our study, however, single oak, pine, and spruce trees were equally bright in these view angles in all wavelength regions except SWIR (Figs. 5, 6, 7).

While, in general, strong anisotropy patterns of spectral reflectance have already earlier been measured for vegetation canopies using both ground-based methods (e.g., Kimes, 1983; Sandmeier and Itten, 1999; Sandmeier et al., 1999; Peltoniemi et al., 2005) and air- and spaceborne sensors (e.g., Ranson et al., 1994; Sandmeier et al., 1999; Rautiainen et al., 2008), in practice, the use of multi-angular reflectance data in monitoring vegetation canopies is not yet common. Empirical evidence, such as that of spectro-directional characteristics of single trees, collected at ground level both outdoors and in laboratory, is essential in understanding the scattering hierarchy within coniferous, broadleaved, and mixed forest canopies, and may improve the reliability of analysis of remote sensing data. Such data are also fundamental in developing and testing physically-based reflectance models.

5. Conclusions

Although empirical data on the spectra of different forest components, such as tree leaves and needles, and of some understory species are nowadays available, the spectro-directional characteristics of individual trees had not been measured before this study. Our results of small trees indicate that simultaneous measurements of both, spectral and directional characteristics of may enhance the discrimination of tree species, and thus may aid in retrieval of information on their biophysical properties. We also described a tree crown level measurement set-up for a goniometer that can, in the future, be applied to collect multi-angular spectra of variety of individual plant species, not only trees.

Data availability

The measurement data are presented in Hovi et al., 2021 (submitted) and are available through Mendeley open access repository.

Declaration of Competing Interest

The authors declare that they have no known competing financial interests or personal relationships that could have appeared to influence the work reported in this paper.

Acknowledgements

This study has received funding from the European Research Council (ERC) under the European Union's Horizon 2020 Research and Innovation Programme (grant agreement No 771049). The text reflects only the authors' view and the Agency is not responsible for any use that may be made of the information it contains. This study was also partly funded by the Academy of Finland project BOREALITY (grant nr 286390). The contribution of M.E.S. is supported by the University of Zurich.

Appendix A. Supplementary data

Supplementary data to this article can be found online at https://doi.org/10.1016/j.rse.2021.112302.

References

Asner, G.P., Braswell, B.H., Schimel, D.S., Wessman, C.A., 1998. Ecological research needs from multiangle remote sensing data. Remote Sens. Environ. 63 (2), 155–165. https://doi.org/10.1016/S0034-4257(97)00139-9.

Atkinson, K., 1982. Numerical integration on the sphere. Journal of the Australian Mathematical Society (Series B) 23, 332–347.

Barnsley, M.J., Lewis, P., O'Dwyer, S., Disney, M.I., Hobson, P., Cutter, M., Lobb, D., 2000. On the potential of CHRIS/PROBA for estimating vegetation canopy properties from space. Remote Sens. Rev. 19, 171–189. https://doi.org/10.1080/02757250009532417.

Barnsley, M.J., Settle, J.J., Cutter, M.A., Lobb, D.R., Teston, F., 2004. The PROBA/CHRIS mission: a low-cost smallsat for hyperspectral multiangle observations of the earth surface and atmosphere. IEEE Trans. Geosci. Remote Sens. 42 (7), 1512–1520. https://doi.org/10.1109/TGRS.2004.827260.

Bicheron, P., Leroy, M., 2000. Bidirectional reflectance distribution function signatures of major biomes observed from space. J. Geophys. Res. 105 (D21) https://doi.org/10.1029/2000JD900380.

Bousquet, L., Lachérade, S., Jacquemoud, S., Moya, I., 2005. Leaf BRDF measurements and model for specular and diffuse components differentiation. Remote Sens. Environ. 98 (2–3), 201–211. https://doi.org/10.1016/j.rse.2005.07.005.

Bréon, F.-M., Vanderbilt, V., Leroy, M., Bicheron, P., Walthall, C.L., Kalshoven, J.E., 1997. Evidence of hot spot directional signature from airborne POLDER measurements. IEEE Trans. Geosci. Remote Sens. 35 (2), 479–484. https://doi.org/10.1109/36.563289.

Canisius, F., Chen, J.M., 2007. Retrieving forest background reflectance in a boreal region from Multi-angle Imaging SpectroRadiometer (MISR) data. Remote Sens. Environ. 107 (1–2), 312–321. https://doi.org/10.1016/j.rse.2006.07.023.

Chen, J.M., Leblanc, S.G., 1997. A four-scale bidirectional reflectance model based on canopy architecture. IEEE Trans. Geosci. Remote Sens. 35 (5), 1316–1337. https://doi.org/10.1109/36.628798.

Chen, J.M., Mo, G., Pisek, J., Liu, J., Deng, F., Ishizawa, M., Chan, D., 2012. Effects of foliage clumping on the estimation of global terrestrial gross primary productivity. Glob. Biogeochem. Cycles 26, GB1019. https://doi.org/10.1029/2010GB003996.

Chianucci, F., Pisek, J., Raabe, K., Marchino, L., Ferrara, C., Corona, P., 2018. A dataset of leaf inclination angles for temperate and boreal broadleaf woody species. Ann. Forest Sci. 75, 50 https://doi.org/10.1007/s13595-018-0730-x.

Dangel, S., Verstraete, M.M., Schopfer, J., Kneubühler, M., Schaepman, M., Itten, K.I., 2005. Toward a direct comparison of field and laboratory goniometer measurements. IEEE Trans. Geosci. Remote Sens. 43 (11), 2666–2675. https://doi.org/10.1109/TGRS.2005.857324.

Daughtry, C.S.T., Biehl, L.L., Ranson, K.J., 1989. A new technique to measure the spectral properties of conifer needles. Remote Sens. Environ. 27 (1), 81–91. https://doi.org/10.1016/0034-4257(89)90039-4.

Deering, D.W., Eck, T.F., Banerjee, B., 1999. Characterization of the reflectance anisotropy of three boreal forest canopies in spring–summer. Remote Sens. Environ. 67 (2), 205–229. https://doi.org/10.1016/S0034-4257(98)00087-X.

Deschamps, P.-Y., Bréon, F.-M., Leroy, M., Podaire, A., Bricaud, A., Buriez, J.-C., Sèze, G., 1994. The POLDER mission: instrument characteristics and scientific objectives. IEEE Trans. Geosci. Remote Sens. 32 (3), 598–599. https://doi.org/10.1109/36.297978.

Diner, D.J., Beckert, J.C., Reilly, T.H., Bruegge, C.J., Conel, J.E., Kahn, R.A., Martonchik, J.V., Ackerman, T.P., Davies, R., Gerstl, S.A.W., Gordon, H.R., Muller, J.-P., Myneni, R.B., Sellers, P.J., Pinty, B., Verstraete, M.M., 1998. Multi-angle Imaging SpectroRadiometer (MISR) instrument description and experiment

overview. IEEE Trans. Geosci. Remote Sens. 36 (4), 1072–1087. https://doi.org/10.1109/36.700992.
Eklundh, L., Hall, K., Eriksson, H., Ardö, J., Pilesjö, P., 2003. Investigating the use of Landsat thematic mapper data for estimation of forest leaf area index in southern Sweden. Can. J. Remote. Sens. 29 (3), 349–362. https://doi.org/10.5589/m03-004.
Farque, L., Sinoquet, H., Colin, F., 2001. Canopy structure and light interception in Quercus petraea seedlings in relation to light regime and plant density. Tree Physiol. 21 (17), 1257–1267. https://doi.org/10.1093/treephys/21.17.1257.
Flower-Ellis, J.G.K., Olsson, L., 1993. Estimation of volume, total and projected area of Scots pine needles from their regression on length. In: Studia Forestalia Suecica, 190.
Forsström, P., Peltoniemi, J., Rautiainen, M., 2019. Seasonal dynamics of lingonberry and blueberry. Silva Fennica 53 (2), 10150. https://doi.org/10.14214/sf.10150.
Gates, D.M., Keegan, H.J., Schleter, J.C., Weidner, V.R., 1965. Spectral properties of plants. Appl. Opt. 4 (1), 11–20. https://doi.org/10.1364/AO.4.000011.
Gerard, F.F., North, P.R.J., 1997. Analyzing the effect of structural variability and canopy gaps on forest BRDF using a geometric-optical model. Remote Sens. Environ. 62 (1), 46–62. https://doi.org/10.1016/S0034-4257(97)00070-9.
Hadi, Korhonen, L., Hovi, A., Rönnholm, P., Rautiainen, M., 2016. The accuracy of large-area forest canopy cover estimation using Landsat in boreal region. Int. J. Appl. Earth Obs. Geoinf. 53, 118–127. https://doi.org/10.1016/j.jag.2016.08.009.
Heiskanen, J., Rautiainen, M., Stenberg, P., Mõttus, M., Vesanto, V.-H., 2013. Sensitivity of narrowband vegetation indices to boreal forest LAI, reflectance seasonality and species composition. ISPRS J. Photogramm. Remote Sens. 78, 1–14. https://doi.org/10.1016/j.isprsjprs.2013.01.001.
Hovi, A., Raitio, P., Rautiainen, M., 2017a. A spectral analysis of 25 boreal tree species. Silva Fennica 51 (4), 7753. https://doi.org/10.14214/sf.7753.
Hovi, A., Lukeš, P., Rautiainen, M., 2017b. Seasonality of albedo and FAPAR in a boreal forest. Agric. For. Meteorol. 247, 331–342. https://doi.org/10.1016/j.agrformet.2017.08.021.
Hovi, A., Forsström, P., Ghielmetti, G., Schaepman, M.E., Rautiainen, M., 2020a. Empirical validation of photon recollision probability in single crowns of tree seedlings. ISPRS J. Photogramm. Remote Sens. 169, 57–72. https://doi.org/10.1016/j.isprsjprs.2020.08.027.
Hovi, A., Mõttus, M., Juola, J., Manoocheri, F., Ikonen, E., Rautiainen, M., 2020b. Evaluating the performance of a double integrating sphere in measurement of reflectance, transmittance, and albedo of coniferous needles. Silva Fennica 54 (2), 10270. https://doi.org/10.14214/sf.10270.
Hovi, A., Forsström, P.R., Ghielmetti, G., Schaepman, M.E., Rautiainen, M., 2021. A Dataset Composed of Multiangular Spectral Libraries and Auxiliary Data at Tree, Leaf, Needle, and Bark Level for Three Common European Tree Species (Submitted to Data in Brief).
Jacquemoud, S., 1993. Inversion of the PROSPECT + SAIL canopy reflectance model from AVIRIS equivalent spectra: theoretical study. Remote Sens. Environ. 44 (2–3), 281–292. https://doi.org/10.1016/0034-4257(93)90022-P.
Juola, J., Hovi, A., Rautiainen, M., 2020. Multiangular spectra of tree bark for common boreal tree species in Europe. Silva Fennica 54 (4), 10331. https://doi.org/10.14214/sf.10331.
Justice, C.O., Townshend, J.R.G., Vermote, E.F., Masuoka, E., Wolfe, R.E., Saleous, N., Roy, D.P., Morisette, J.T., 2002. An overview of MODIS land data processing and product status. Remote Sens. Environ. 83, 3–15. https://doi.org/10.1016/S0034-4257(02)00084-6.
Kimes, D.S., 1983. Dynamics of directional reflectance factor distributions for vegetation canopies. Appl. Opt. 22 (9), 1364–1372. https://doi.org/10.1364/AO.22.001364.
Kimes, D.S., Newcomb, W.W., Nelson, R.F., Schutt, J.B., 1986. Directional reflectance distributions of a hardwood and pine forest canopy. IEEE Trans. Geosci. Remote Sens. GE-24 (2), 281–293. https://doi.org/10.1109/TGRS.1986.289647.
Knipling, E.B., 1970. Physical and physiological basis for the reflectance of visible and near-infrared radiation from vegetation. Remote Sens. Environ. 1 (3), 155–159. https://doi.org/10.1016/S0034-4257(70)80021-9.
Knyazikhin, Y., Martonchik, J.V., Diner, D.J., Myneni, R.B., Verstraete, M., Pinty, B., Gobron, N., 1998. Estimation of vegetation canopy leaf area index and fraction of absorbed photosynthetically active radiation from atmosphere-corrected MISR data. J. Geophys. Res. 103 (D24), 32239–32256. https://doi.org/10.1029/98JD02461.
Kobayashi, H., Iwabuchi, H., 2008. A coupled 1-D atmosphere and 3-D canopy radiative transfer model for canopy reflectance, light environment, and photosynthesis simulation in a heterogeneous landscape. Remote Sens. Environ. 112 (1), 173–185. https://doi.org/10.1016/j.rse.2007.04.010.
Korhonen, L., Korpela, I., Heiskanen, J., Maltamo, M., 2011. Airborne discrete-return LIDAR data in the estimation of vertical canopy cover, angular canopy closure and leaf area index. Remote Sens. Environ. 115 (4), 1065–1080. https://doi.org/10.1016/j.rse.2010.12.011.
Korpela, I., Heikkinen, V., Honkavaara, E., Rohrbach, F., Tokola, T., 2011. Variation and directional anisotropy of reflectance at the crown scale – implications for tree species classification in digital aerial images. Remote Sens. Environ. 115, 2062–2074. https://doi.org/10.1016/j.rse.2011.04.008.
Korpela, I., Mehtätalo, L., Markelin, L., Seppänen, A., Kangas, A., 2014. Tree species identification in aerial image data using directional reflectance signatures. Silva Fennica 48 (3), 1087. https://doi.org/10.14214/sf.1087.
Kuusinen, N., Juola, J., Karki, B., Stenroos, S., Rautiainen, M., 2020. A spectral analysis of common boreal ground lichen species. Remote Sens. Environ. 247, 111955. https://doi.org/10.1016/j.rse.2020.111955.
Kuusk, A., Kuusk, J., Lang, M., 2014. Modeling directional forest reflectance with the hybrid type forest reflectance model FRT. Remote Sens. Environ. 149, 196–204. https://doi.org/10.1016/j.rse.2014.03.035.
Kuusk, A., Pisek, J., Lang, M., Märdla, S., 2018. Estimation of gap fraction and foliage clumping in forest canopies. Remote Sens. 10 (7), 1153. https://doi.org/10.3390/rs10071153.
Lacaze, R., Roujean, J.-L., 2001. G-function and HOt SpoT (GHOST) reflectance model: application to multi-scale airborne POLDER measurements. Remote Sens. Environ. 76 (1), 67–80. https://doi.org/10.1016/S0034-4257(00)00193-0.
Li, X., Strahler, A.H., 1992. Geometric-optical bidirectional reflectance modeling of the discrete crown vegetation canopy: effect of crown shape and mutual shadowing. IEEE Trans. Geosci. Remote Sens. 30 (2), 276–292. https://doi.org/10.1109/36.134078.
Lobell, D.B., Asner, G.P., Law, B.E., Treuhaft, R.N., 2002. View angle effects on canopy reflectance and spectral mixture analysis of coniferous forests using AVIRIS. Int. J. Remote Sens. 23 (11), 2247–2262. https://doi.org/10.1080/01431160110075613.
Lunagaria, M.M., Patel, H.R., 2017. Changes in reflectance anisotropy of wheat crop during different phenophases. Int. Agrophys. 31 (2), 203–218. https://doi.org/10.1515/intag-2016-0045.
Markiet, V., Hernández-Clemente, R., Mõttus, M., 2017. Spectral similarity and PRI variations for a boreal forest stand using multi-angular airborne imagery. Remote Sens. 9 (10), 1005. https://doi.org/10.3390/rs9101005.
Mõttus, M., Rautiainen, M., Schaepman, M.E., 2012. Shoot scattering phase function for Scots pine and its effect on canopy reflectance. Agric. For. Meteorol. 154–155, 67–74. https://doi.org/10.1016/j.agrformet.2011.10.012.
Otsu, N., 1979. A threshold selection method from gray-level histograms. IEEE Trans. Syst. Man Cybernet. 9 (1), 62–66. https://doi.org/10.1109/TSMC.1979.4310076.
Peltoniemi, J.I., Kaasalainen, S., Näränen, J., Rautiainen, M., Stenberg, P., Smolander, H., Smolander, S., Voipio, P., 2005. BRDF measurement of understory vegetation in pine forests: dwarf shrubs, lichen, and moss. Remote Sens. Environ. 94 (3), 343–354. https://doi.org/10.1016/j.rse.2004.10.009.
Pisek, J., Chen, J.M., Kobayashi, H., Rautiainen, M., Schaepman, M.E., Karnieli, A., Sprinstin, M., Ryu, Y., Nikopensius, M., Raabe, K., 2016. Retrieval of seasonal dynamics of forest understory reflectance from semiarid to boreal forests using MODIS BRDF data. J. Geophys. Res. 121, 855–863. https://doi.org/10.1002/2016JG003322.
Ranson, K.J., Irons, J.R., Williams, D.L., 1994. Multispectral bidirectional reflectance of northern forest canopies with the Advanced Solid-State Array Spectroradiometer (ASAS). Remote Sens. Environ. 47, 276–289. https://doi.org/10.1016/0034-4257(94)90161-9.
Rautiainen, M., Lukeš, P., 2015. Spectral contribution of understory to forest reflectance in a boreal site: an analysis of EO-1 Hyperion data. Remote Sens. Environ. 171, 98–104. https://doi.org/10.1016/j.rse.2015.10.009.
Rautiainen, M., Stenberg, P., Nilson, T., Kuusk, A., 2004. The effect of crown shape on the reflectance of coniferous stands. Remote Sens. Environ. 89 (1), 41–52. https://doi.org/10.1016/j.rse.2003.10.001.
Rautiainen, M., Lang, M., Mõttus, M., Kuusk, A., Nilson, T., Kuusk, J., Lükk, T., 2008. Multi-angular reflectance properties of a hemiboreal forest: an analysis using CHRIS PROBA data. Remote Sens. Environ. 112 (5), 2627–2642. https://doi.org/10.1016/j.rse.2007.12.005.
Rautiainen, M., Mõttus, M., Heiskanen, J., Akujärvi, A., Majasalmi, T., Stenberg, P., 2011. Seasonal reflectance dynamics of common understory types in a northern European boreal forest. Remote Sens. Environ. 115 (12), 3020–3028. https://doi.org/10.1016/j.rse.2011.06.005.
Rautiainen, M., Mõttus, M., Yáñez-Rausell, L., Homolová, L., Malenovský, Z., Schaepman, M.E., 2012. A note on upscaling coniferous needle spectra to shoot spectral albedo. Remote Sens. Environ. 117, 469–474. https://doi.org/10.1016/j.rse.2011.10.019.
Roosjen, P.P.J., Clevers, J.G.P.W., Bartholomeus, H.M., Schaepman, M.E., Schaepman-Strub, G., Jalink, H., Van der Schoor, R., De Jong, A., 2012. A laboratory goniometer system for measuring reflectance and emittance anisotropy. Sensors 12, 17358–17371. https://doi.org/10.3390/s121217358.
Roosjen, P.P.J., Suomalainen, J.M., Bartholomeus, H.M., Kooistra, L., Clevers, J.G.P.W., 2017. Mapping reflectance anisotropy of a potato canopy using aerial images acquired with an unmanned aerial vehicle. Remote Sens. 9 (5), 417. https://doi.org/10.3390/rs9050417.
Roosjen, P.P.J., Brede, B., Suomalainen, J.M., Bartholomeus, H.M., Kooistra, L., Clevers, J.G.P.W., 2018. Improved estimation of leaf area index and leaf chlorophyll content of a potato crop using multi-angle spectral data – potential of unmanned aerial vehicle imagery. Int. J. Appl. Earth Obs. Geoinf. 66, 14–26. https://doi.org/10.1016/j.jag.2017.10.012.
Roujean, J.-L., Leroy, M., Deschamps, P.-Y., 1992. A bidirectional reflectance model of the Earth's surface for the correction of remote sensing data. J. Geophys. Res. 97 (D18), 20455–20468. https://doi.org/10.1029/92JD01411.
Rouse Jr., J.W., Haas, R.H., Schell, J.A., Deering, D.W., 1974. Monitoring vegetation systems in the Great Plains with ERTS. NASA, Goddard Space Flight Center Third ERTS-1 Symposium 1 (A), 309–317.
Sandmeier, St., Deering, D.W., 1999. Structure analysis and classification of boreal forests using airborne hyperspectral BRDF data from ASAS. Remote Sens. Environ. 69 (3), 281–295. https://doi.org/10.1016/S0034-4257(99)00032-2.
Sandmeier, S.R., Itten, K.I., 1999. A field goniometer system (FIGOS) for acquisition of hyperspectral BRDF data. IEEE Trans. Geosci. Remote Sens. 37 (2), 978–986. https://doi.org/10.1109/36.752216.
Sandmeier, S.R., Middleton, E.M., Deering, D.W., Qin, W., 1999. The potential of hyperspectral bidirectional reflectance distribution function data for grass canopy characterization. J. Geophys. Res. 104 (D8), 9547–9560. https://doi.org/10.1029/1999JD900094.

Schaepman-Strub, G., Schaepman, M.E., Painter, T.H., Dangel, S., Martonchik, J.V., 2006. Reflectance quantities in optical remote sensing – definitions and case studies. Remote Sens. Environ. 103 (1), 27–42. https://doi.org/10.1016/j.rse.2006.03.002.

Schneider, F.D., Leiterer, R., Morsdorf, F., Gastellu-Etchegorry, J.P., Lauret, N., Pfeifer, N., Schaepman, M.E., 2014. Simulating imaging spectrometer data: 3D forest modeling based on LiDAR and in situ data. Remote Sens. Environ. 152, 235–250. https://doi.org/10.1016/j.rse.2014.06.015.

Schopfer, J., Dangel, S., Kneubühler, M., Itten, K.I., 2008. The improved dual-view field goniometer system FIGOS. Sensors 8 (8), 5120–5140. https://doi.org/10.3390/s8085120.

Sellin, A., 2000. Estimating the needle area from geometric measurements: application of different calculation methods to Norway spruce. Trees 14, 215–222. https://doi.org/10.1007/PL00009765.

Stenberg, P., Mõttus, M., Rautiainen, M., Sievänen, R., 2014. Quantitative characterization of clumping in Scots pine crowns. Ann. Bot. 114 (4), 689–694. https://doi.org/10.1093/aob/mct310.

Verrelst, J., Schaepman, M.E., Koetz, B., Kneubühler, M., 2008. Angular sensitivity analysis of vegetation indices derived from CHRIS/PROBA data. Remote Sens. Environ. 112, 2341–2353. https://doi.org/10.1016/j.rse.2007.11.001.

Verrelst, J., Schaepman, M.E., Clevers, J.G.P.W., 2010. Spectrodirectional Minnaert-k retrieval using CHRIS-PROBA data. Can. J. Remote. Sens. 36 (6), 631–644. https://doi.org/10.5589/m11-012.